Stereochemical Non-rigidity of Dithioether Complexes of Trimethylplatinum(IV) Halides. *X*-Ray Crystal Structures of [$PtClMe_3(MeSCH_2CH_2SEt)$] and [$PtIMe_3(MeSCH_2CH_2SBu^t)$] *

Edward W. Abel, Ian Moss, Keith G. Orrell, Vladimir Šik, and David Stephenson
Department of Chemistry, University of Exeter, Exeter EX4 4QD
Paul A. Bates and Michael B. Hursthouse
Department of Chemistry, Queen Mary College, Mile End Road, London E1 4NS

Platinum(IV) complexes of general type [$PtXMe_3(RSCH_2CH_2SR')$] (X = Cl, Br, or I; R = Me, R' = Et or Bu^t; R = R' = Bu^t) have been synthesised. Solid-state structures for two of the complexes (X = Cl, R = Me, R' = Et; X = I, R = Me, R' = Bu^t) have been established by *X*-ray crystallography. All the complexes have been extensively studied in solution by variable-temperature one- and two-dimensional n.m.r. spectroscopy. The thioalkyl dependence of the energy barriers for pyramidal sulphur inversion was found to be SMe > SEt ≫ SBu^t. At above-ambient temperatures ligand 180° rotations and $PtMe_3$ 120° rotations occur, these two fluxions showing high degrees of correlation.

Some years ago we reported on the syntheses[1] and dynamic structural properties[2] of trimethylplatinum(IV) halide complexes with dithio- and diseleno-ethers of type [$PtXMe_3(MeECH_2CH_2EMe)$] (X = Cl, Br, or I; E = S or Se). These complexes possess interesting dynamic stereochemistries, which were the subject of detailed n.m.r. studies.[3] This early work formed the basis of subsequent investigations on related complexes of type [$PtXMe_3L$] (X = Cl, Br, or I; L = $MeECH_2CH_2CH_2EMe$,[1,2] *cis*-$MeECH{=}CHEMe$,[4] *o*-$MeEC_6H_4EMe$,[5] or $MeSCH_2SCH_2SMe$[6]). All these chelate complexes, in organic solvents, exist as mixtures of isomers (invertomers) arising from the relative dispositions of the E-methyl groups. At low temperatures n.m.r. spectra reveal three distinct invertomer species, namely *meso*-1, *meso*-2, and a DL-1/2 pair. The relative populations of these species vary considerably with the halogen, X, and the ligand, L. The chalcogen inversion energies, as measured by total n.m.r. bandshape analyses, have been shown to be influenced by both ligand ring size[1,2,6] and backbone nature.[4,5]

We have now sought to investigate the sulphur inversion energy dependence on the attached alkyl group, by synthesising the unsymmetrical dithioether ligand complexes [$PtXMe_3(RSCH_2CH_2SR')$] (X = Cl, Br, or I; R = Me, R' = Et or Bu^t), together with the symmetrical complexes [$PtXMe_3(Bu^tSCH_2CH_2SBu^t)$]. Apart from a study of [$PtXMe_3(MeSCH_2CH_2SeMe)$],[5] investigations of unsymmetrical thioether ligand complexes have not been attempted to date, on account of the almost insuperable difficulties in analysing their ^1H dynamic n.m.r. spectra. These problems arise from the fact that the spectra are the outcome of exchange between four n.m.r.-distinct species (DL-1 to DL-4), spectra at each temperature being characterised by up to six independent rate constants.

Recently, however, we have shown how very reliable rate data can be extracted from two-dimensional n.m.r. exchange studies (2D-EXSY)[7] and have described the case of [$PtIMe_3(MeSCH_2CH_2SEt)$] in detail.[8] We have now applied a combination of one-dimensional bandshape and 2D-EXSY experiments to related Pt^{IV} complexes, and report here on the trends in ground-state invertomer populations, sulphur inversion energies, and ligand rotation/Pt-methyl scrambling energies throughout the series [$PtXMe_3L$] (X = Cl, Br, or I; L = $MeSCH_2CH_2SMe$, $MeSCH_2CH_2SEt$, $MeSCH_2CH_2SBu^t$, or $Bu^tSCH_2CH_2SBu^t$). For two of the complexes, (X = Cl, L = $MeSCH_2CH_2SEt$) and (X = I, L = $MeSCH_2CH_2SBu^t$), the ground-state solution structures are compared with the solid-state *X*-ray crystal structures.

Experimental

Synthesis of Ligands.—2,2,7,7-*Tetramethyl*-3,6-*dithiaoctane*, $Bu^tSCH_2CH_2SBu^t$. This was prepared by a literature method.[9] An additional quantity was subsequently obtained from K & K Chemicals Ltd.

6,6-*Dimethyl*-2,5-*dithiaheptane*, $MeSCH_2CH_2SBu^t$. Sodium metal (3.5 g, 0.15 mol) was dissolved in methanol (250 cm^3) under nitrogen and 2-methyl-2-propanethiol (13.7 g, 0.15 mol) added quickly *via* a pressure-equalising dropping funnel. The mixture was stirred at room temperature for 1 h, and 2-chloroethyl methyl sulphide (16.8 g, 0.15 mol) added dropwise over a period of 30 min. The mixture was stirred for 16 h, after which the volume of the solution was reduced to *ca.* 50 cm^3 by rotary evaporation. After filtration, the product was isolated by distillation at reduced pressure, the fraction boiling at 58—60 °C (0.1 mmHg pressure) being collected. The yield of the required product was 18.0 g (72%). ^1H N.m.r. ($CDCl_3$): δ 1.37 (s, CMe_3), 2.18 (s, SMe), 2.76 (s, SCH_2CH_2S).

2,5-*Dithiaheptane*, $MeSCH_2CH_2SEt$. This was prepared as above, employing ethanethiol in place of 2-methyl-2-propanethiol. Yield for the same scale preparation was 7.8 g (38.0%). B.p. 75—76 °C (0.1 mmHg). ^1H N.m.r. ($CDCl_3$ solution): δ 1.25 (t, $^3J_{HH}$ = 7.46 Hz, SCH_2CH_3), 2.13 (s, SMe), 2.55 (q, $^3J_{HH}$ = 7.46 Hz, SCH_2CH_3), 2.72 (s, SCH_2CH_2S).

Trimethylplatinum(IV) *Halide Complexes of Dithioether Ligands.*—All complexes were synthesised by the thermal reaction of [$(PtXMe_3)_4$] (X = Cl, Br, or I) with the appropriate ligand in chloroform according to published procedures.[1] One typical example of the method is as follows.

[$(PtBrMe_3)_4$] (0.24 g, 0.75 mmol, based on the monomeric $PtBrMe_3$ unit) and $Bu^tSCH_2CH_2SBu^t$ (0.31 g, 1.50 mmol) were heated under reflux for 3 h in $CDCl_3$ (*ca.* 50 cm^3). After cooling and removal of solvent at reduced pressure, a colourless oil was obtained. This was extracted with hexane (10 cm^3) to remove excess ligand, and a white solid was isolated. Recrystallisation

* Chloro(2,5-dithiaheptane-*SS'*)- and (6,6-dimethyl-2,5-dithiaheptane-*S*^{2})iodo-trimethylplatinum(IV) respectively.

Supplementary data available: see Instructions for Authors, *J. Chem. Soc., Dalton Trans.*, 1988, Issue 1, pp. xvii—xx.

Non-S.I. unit employed: mmHg ≈ 133 Pa.

Table 1. Syntheses, analytical data, and melting points for the complexes *fac*-[$PtXMe_3(L\text{–}L)$] (X = Cl, Br, or I; L–L = chelating dithioether)

Complex	Yield[a] (%)	Melting point[b] (°C)	Analysis (%) Found C	Found H	Calculated C	Calculated H
fac-[$PtClMe_3(Bu^tSCH_2CH_2SBu^t)$]	51.8	111—112	32.2	6.6	32.4	6.5
fac-[$PtBrMe_3(Bu^tSCH_2CH_2SBu^t)$]	58.7	117—118	29.8	6.1	29.7	5.9
fac-[$PtIMe_3(Bu^tSCH_2CH_2SBu^t)$]	52.8	125—127	27.5	5.7	27.2	5.5
fac-[$PtClMe_3(MeSCH_2CH_2SBu^t)$]	74.6	94—95	27.2	5.7	27.3	5.7
fac-[$PtBrMe_3(MeSCH_2CH_2SBu^t)$]	39.2	110—111	24.7	5.3	24.8	5.2
fac-[$PtIMe_3(MeSCH_2CH_2SBu^t)$]	39.8	129—130	22.5	4.6	22.6	4.7
fac-[$PtClMe_3(MeSCH_2CH_2SEt)$]	50.0	86—87	23.3	5.1	23.3	5.1
fac-[$PtBrMe_3(MeSCH_2CH_2SEt)$]	43.5	91—92	21.0	4.7	21.1	4.6
fac-[$PtIMe_3(MeSCH_2CH_2SEt)$]	53.7	98—99	19.1	4.3	19.1	4.2

[a] Yields are quoted relative to $[(PtXMe_3)_4]$. [b] Uncorrected.

from chloroform–hexane afforded colourless *crystals* of *fac*-[$PtBrMe_3(Bu^tSCH_2CH_2SBu^t)$] {yield 0.23 g, 58.7% based on $[(PtBrMe_3)_4]$}.

Yields, melting points, and analytical data for these complexes, all of which were colourless crystalline solids, are given in Table 1. Elemental analyses were performed by Butterworth Laboratories Ltd., London.

N.M.R. Spectra.—Hydrogen-1, ^{13}C-{^1H}, and ^{195}Pt-{^1H} n.m.r. spectra were recorded on a Bruker AM250 FT spectrometer operating at 250.13, 62.90, and 53.53 MHz respectively. A standard B-VT1000 variable-temperature unit was used to control the probe temperature, the calibration of this unit being checked periodically against a Comark digital thermometer. Quoted temperatures are considered accurate to ±1 °C.

Hydrogen-1 and ^{195}Pt-{^1H} 2D-EXSY spectra were recorded as previously reported[7,8] using the Bruker automation programs NOESY and NOESYX respectively. For the ^{195}Pt experiments the F1 dimension of the data table contained 128 words which was then zero-filled to 512 words. For the ^1H two-dimensional experiments, the F1 dimension contained 64 words, zero-filled to 512 words. In all experiments the F2 dimension contained 1 024 words. No random variation of the mixing time, τ_m, was provided since no scalar couplings were present. The number of scans per experiment was in the range 72—184 for ^{195}Pt and 4 for ^1H, giving total experiment times of *ca.* 15 h and 1 h respectively. Data relating to spectra at temperatures below 273 K were processed using an unshifted sine-bell window function in both dimensions. At temperatures above 273 K, no window functions were used in the data processing. In all cases, magnitude mode spectra were calculated, and symmetrised about the diagonal.

N.M.R. Computations.—The dynamic information was extracted from the one-dimensional spectra by total bandshape analysis using a modified version of the DNMR program of Kleier and Binsch.[10] The dynamic information contained in the cross-peak signals of the ^{195}Pt-{^1H} and ^1H 2D-EXSY spectra was processed using the D2DNMR program described previously.[7] Choices of optimal mixing times, τ_m, were based on the experience gained in the previous studies of [$PtXMe_3(MeSCH_2CH_2SMe)$][7] and [$PtIMe_3(MeSCH_2CH_2SEt)$].[8]

X-*Ray Structure Determinations.*—Single-crystal structure determinations of [$PtClMe_3(MeSCH_2CH_2SEt)$] (**1**) and [$PtIMe_3(MeSCH_2CH_2SBu^t)$] (**2**) were carried out.

Crystal data for (**1**). $C_8H_{21}ClPtS_2$, M = 411.917, orthorhombic, space group *Pbca*, a = 10.979(2), b = 12.402(3), c = 19.624(2) Å, U = 2 672(1) Å^3, Z = 8, D_c = 2.048 g cm^{-3}, $F(000)$ = 1 568, λ = 0.710 69 Å, $\mu(Mo\text{-}K_\alpha)$ = 110.7 cm^{-1}, crystal size 0.63 × 0.63 × 0.20 mm.

Crystal data for (**2**). $C_{10}H_{25}IPtS_2$, M = 531.422, monoclinic, space group $P2_1/n$, a = 13.329(2), b = 8.355(1), c = 15.529(2) Å, β = 113.79(1)°, U = 1 582.5(4) Å^3, Z = 4, D_c = 2.231 g cm^{-3}, $F(000)$ = 992, λ = 0.710 69 Å, $\mu(Mo\text{-}K_\alpha)$ = 111.2 cm^{-1}, crystal size 0.63 × 0.40 × 0.38 mm.

Data collection. For both (**1**) and (**2**) unit-cell parameters and intensity data were obtained by following previously detailed procedures,[11] using a CAD4 diffractometer operating in the ω–2θ scan mode, with graphite-monochromated Mo-K_α radiation.

For (**1**) a total of 2 355 unique reflections were collected ($3 \leqslant 2\theta \leqslant 50°$). The segment of reciprocal space scanned was: h, 0—13; k, 0—14; l, 0—23. The reflection intensities were corrected for absorption, using the azimuthal-scan method;[12] maximum and minimum transmission factors 1.00, 0.42.

For (**2**) a total of 2 774 unique reflections were collected ($3 \leqslant 2\theta \leqslant 50°$). The segment of reciprocal space scanned was: h, −15—15; k, 0—9; l, 0—18. These reflections were also corrected for absorption;[12] maximum and minimum transmission factors 1.00, 0.75.

Solution and refinement of structures. Both structures were solved by the application of routine heavy-atom methods (SHELX-86[13]), and refined by full-matrix least-squares (SHELX-76[14]). All non-hydrogen atoms were refined anisotropically, and hydrogen atoms placed into calculated positions (C–H 0.96 Å, U = 0.10 Å^2).

For (**1**) the final residuals R and R' were 0.032 and 0.034 respectively for the 124 variables and 1 550 data for which $F_o \geqslant 6\sigma(F_o)$. For (**2**) the final residuals were 0.027 and 0.026 for 148 variables and 2 397 data [$F_o > 6\sigma(F_o)$]. The function minimised in each case was $\Sigma w(|F_o| - |F_c|)^2$, with the weight, w, being defined as $1/[\sigma^2(F_o) + gF_o^2]$ [g = 0.0002 for (**1**) and 0.000 001 for (**2**)].

Atomic scattering factors and anomalous scattering parameters were taken from refs. 15 and 16 respectively. All computations were made on a DEC VAX-11/750 computer.

Results

Trimethylplatinum(IV) *Halide Derivatives of* 2,5-*Dithiaheptane.*—The fluxional behaviour of the complexes [$PtXMe_3(MeSCH_2CH_2SEt)$] in solution has been examined in some

Table 2. Fractional atomic co-ordinates ($\times 10^4$) for *fac*-[$PtClMe_3$-($MeSCH_2CH_2SEt$)]

Atom	*x*	*y*	*z*
Pt	−1 267.5(4)	7 758.1(3)	8 941.1(2)
Cl	−1 731(3)	6 630(2)	7 934(2)
S(1)	870(3)	7 215(3)	8 969(2)
S(2)	−676(3)	9 105(2)	8 095(2)
C(1)	−3 044(11)	8 297(10)	8 957(6)
C(2)	−1 805(10)	6 575(8)	9 610(6)
C(3)	−929(10)	8 690(8)	9 782(5)
C(4)	1 536(11)	8 238(11)	8 443(9)
C(5)	725(13)	8 591(11)	7 849(7)
C(6)	1 149(12)	6 027(9)	8 444(7)
C(7)	822(14)	5 048(12)	8 812(8)
C(8)	−277(12)	10 368(8)	8 480(6)

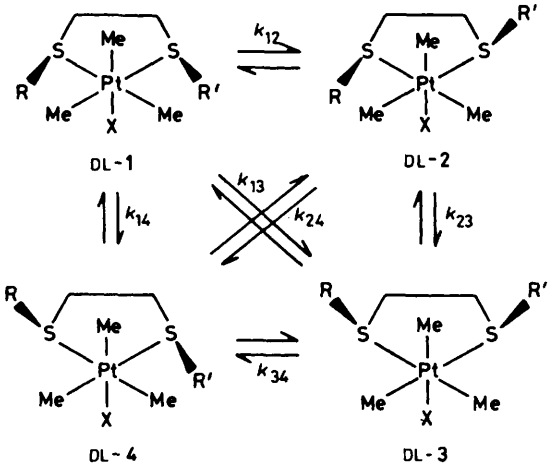

Figure 1. The four invertomers of [$PtXMe_3(RSCH_2CH_2SR')$] (X = Cl, Br, or I; R = Me, R' = Et or Bu^t) and their interconversions by single-site and double-site sulphur inversion (*N.B.* only individual members of the DL pairs are shown). When R = R' = Me or Bu^t, DL-1 and DL-3 species become *meso*-1 and *meso*-2, respectively, and DL-2 and DL-4 become a mirror-image DL pair

detail. Conventional one-dimensional n.m.r. bandshape methods were, however, unable to handle the complexities of the exchange-broadened spectra arising from pyramidal sulphur inversion, since such spectra were sensitive to at least four independent rate constants arising from the interconversion of the four DL invertomer species (Figure 1). Additionally, high-temperature ligand switching and trimethylplatinum fluxions were characterised by a further three rate constants. Dynamic spin systems of such complexities can, however, be evaluated without undue difficulty by 2D-EXSY experiments.[7] Before considering the results of these experiments, however, the *X*-ray crystal structure of [$PtClMe_3(MeSCH_2CH_2SEt)$] is described, and this structure compared to the pseudostatic solution structures of all three dithiaheptane complexes.

X-*Ray Crystal Structure of* fac-[$PtClMe_3(MeSCH_2CH_2$-SEt)].—The structure, with the atomic labelling scheme, is shown in Figure 2. Fractional atomic co-ordinates and selected bond lengths and angles are collected in Tables 2 and 3, respectively. The co-ordination about the platinum centre is approximately octahedral, with bond angles in the ranges 84.2—96.5 and 176.4—178.6°. The thioalkyl groups adopt a mutually *anti* orientation relative to the chelate ring, with the ethyl group *cis* to chloride. This structure closely resembles the DL-4 invertomer

Table 3. Bond lengths (Å) and angles (°) for *fac*-[$PtClMe_3$-($MeSCH_2CH_2SEt$)] *

(*i*) Bond lengths			
Cl–Pt	2.474(5)	S(1)–Pt	2.442(5)
S(2)–Pt	2.443(5)	C(1)–Pt	2.061(14)
C(2)–Pt	2.055(11)	C(3)–Pt	2.048(12)
C(4)–S(1)	1.792(17)	C(6)–S(1)	1.824(13)
C(5)–S(2)	1.734(16)	C(8)–S(2)	1.793(12)
C(5)–C(4)	1.530(21)	C(7)–C(6)	1.457(19)
(*ii*) Bond angles			
S(1)–Pt–Cl	93.4(2)	S(2)–Pt–Cl	84.2(2)
S(2)–Pt–S(1)	87.1(2)	C(1)–Pt–Cl	90.1(4)
C(1)–Pt–S(1)	176.4(3)	C(1)–Pt–S(2)	92.3(4)
C(2)–Pt–Cl	92.7(4)	C(2)–Pt–S(1)	93.7(4)
C(2)–Pt–S(2)	176.8(3)	C(2)–Pt–C(1)	87.1(6)
C(3)–Pt–Cl	178.6(3)	C(3)–Pt–S(1)	87.9(4)
C(3)–Pt–S(2)	96.5(4)	C(3)–Pt–C(1)	88.7(5)
C(3)–Pt–C(2)	86.6(6)	C(4)–S(1)–Pt	100.6(6)
C(6)–S(1)–Pt	111.8(5)	C(6)–S(1)–C(4)	100.2(7)
C(5)–S(2)–Pt	100.0(5)	C(8)–S(2)–Pt	112.1(5)
C(8)–S(2)–C(5)	102.7(8)	C(5)–C(4)–S(1)	113.9(10)
C(4)–C(5)–S(2)	114.2(10)	C(7)–C(6)–S(1)	110.6(11)

* Values in parentheses are the estimated standard deviations of the least significant figure.

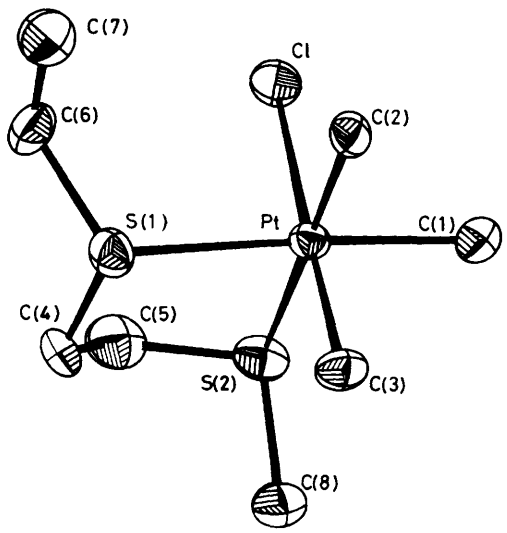

Figure 2. Crystal structure of *fac*-[$PtClMe_3(MeSCH_2CH_2SEt)$] showing the atomic labelling

detected in solution (Figure 1). The slight distortion from pseudo-octahedral co-ordination is illustrated by the angles C(3)–Pt–S(2) and S(1)–Pt–Cl being 96.5 and 93.4° respectively, *i.e.* axial ligand–platinum–sulphur bond angles are >90° when the sulphur atom bears a thioalkyl group *cis* to the axial ligand. The Pt–S bond lengths are identical at 2.443 Å. This value compares with those of 2.458 and 2.473 Å for [$(PtClMe_3)_2(SCH_2SCH_2SCH_2)$],[17] 2.475 Å for [$(PtClMe_3)_2$-$(SCH_2SCH_2SCH_2SCH_2)$],[18] and 2.465 Å for Pt^{IV}–S bonds in [(dppe)$Pt(\mu$-$SMe)_2PtClMe_3$],[19] indicating slightly stronger bonds in the present complex. In this case the bulkier ethyl group does not appear to cause any lengthening (and hence weakening) of the associated Pt–S bond. The Pt–C bond lengths which average to 2.058 (*trans* S) and 2.048 Å (*trans* Cl) are not

Table 4. ^{195}Pt-{^{1}H} N.m.r. chemical shifts (δ)[a] and invertomer populations (*p*)[b] of the complexes [$PtXMe_3(MeSCH_2CH_2SR)$]

Complex	DL-1/*meso*-1[c] δ	DL-1/*meso*-1[c] *p*	DL-2 δ	DL-2 *p*	DL-4 δ	DL-4 *p*	DL-3/*meso*-2[c] δ	DL-3/*meso*-2[c] *p*
[$PtClMe_3(MeSCH_2CH_2SEt)$]	1 372.8[d]	53.0	1 360.4[d]	20.7	1 358.1[d]	23.3	1 334.4[d]	2.9
[$PtBrMe_3(MeSCH_2CH_2SEt)$]	1 267.5	41.4	1 237.1	24.0	1 229.1	28.6	1 193.7	5.9
[$PtIMe_3(MeSCH_2CH_2SEt)$]	1 082.2	26.0	1 031.4	27.4	1 014.5	36.1	964.6	10.5
[$PtClMe_3(MeSCH_2CH_2SMe)$][e]	1 362.0	59.5	1 348.2	19.0	1 348.2	19.0	1 319.4	2.5
[$PtBrMe_3(MeSCH_2CH_2SMe)$][e]	*f*	35.8	*f*	29.5	*f*	29.5	*f*	5.4
[$PtIMe_3(MeSCH_2CH_2SMe)$][e]	1 086.4	29.5	1 019.5	30.3	1 019.5	30.3	951.0	10.0

[a] Shifts at 243 K, relative to ^{195}Pt Ξ = 21.4 MHz. [b] Percentage populations at 243 K. [c] For 2,5-dithiahexane complexes. [d] At 253 K. [e] Ref. 7. [f] Not measured.

Table 5. Carbon-13 n.m.r. parameters for complexes [$PtXMe_3(MeSCH_2CH_2SEt)$] in $CDCl_3$ at −30 °C (platinum-methyl signals)[a]

X	DL-1 Axial	DL-1 Equatorial	DL-2 Axial	DL-2 Equatorial	DL-4 Axial	DL-4 Equatorial
Cl	−4.63 (694.8)	−0.38 (640.9)[b] −1.12 (639.9)[c]	−5.84 (705.8)	−0.49 (627.8)[b] −1.66 (631.0)[c]	−5.11 (705.9)	−0.57 (630.6)[b] −1.24 (630.3)[c]
Br	−0.26 (687.3)	−1.01 (635.1)[b] −1.91 (633.8)[c]	−1.70 (698.5)	−1.34 (622.9)[b] −2.42 (625.8)[c]	−0.97 (697.5)	−1.51 (624.1)[b] −1.97 (626.6)[c]
I	6.20 (665.2)	−2.38 (626.0)[b] −3.36 (623.6)[c]	4.43 (676.0)	−3.29 (615.0)[b] −3.93 (617.5)[c]	5.18 (675.8)	−3.46 (617.2)[b] −3.63 (615.2)[c]

[a] Chemical shifts (δ), values in parentheses are ^{1}J(PtC)/Hz. Signals for the DL-3 invertomer were not observed. [b] *trans* to SMe. [c] *trans* to SEt.

Table 6. Carbon-13 n.m.r. parameters (ligand signals)[a] for complexes [$PtXMe_3(MeSCH_2CH_2SEt)$] in $CDCl_3$ at −30 °C

X	Assignment	DL-1	DL-2	DL-3	DL-4
	SMe	14.84	14.67	12.53	11.23 (7.8)
	SCH_2CH_3	11.80	11.55		11.64
Cl	SCH_2CH_3	26.53	22.91	24.16	25.90
	$MeSCH_2CH_2SEt$	32.07	32.84[b]		31.81[b]
	$MeSCH_2CH_2SEt$	35.47	34.70		35.24
	SMe	16.57 (6.6)	16.80 (8.2)	12.63	11.28 (8.2)
	SCH_2CH_3	11.74	11.77[b]		11.98[b]
Br	SCH_2CH_3	28.48	23.11	24.24	27.93 (6.6)
	$MeSCH_2CH_2SEt$	32.36	33.08[b]		32.15[b]
	$MeSCH_2CH_2SEt$	35.88	35.01		35.53
	SMe	20.25 (7.9)	21.07 (9.1)	12.72	11.37 (7.1)
	SCH_2CH_3	11.81 (4.6)	12.41 (6.9)	11.73	12.13 (5.1)
I	SCH_2CH_3	32.21 (7.5)	23.22	24.27	31.82 (8.2)
	$MeSCH_2CH_2SEt$	32.73	33.24	33.42	32.69
	$MeSCH_2CH_2SEt$	36.42	35.46		35.82

[a] Chemical shifts (δ); values in parentheses are ^{2}J(PtC) (SMe and methylene signals) or ^{3}J(PtC) (SCH_2CH_3 signals) in Hz. [b] Assignments of DL-2 and DL-4 signals are uncertain.

substantially different from previously reported structures. The C(ligand backbone)–S–Pt bond angles are identical (within error limits) at 100.3°, as are the C(alkyl)–S–Pt angles (110.0°). The chelate ring conformation is similar to that reported for other 1,2-bis(alkylthio)ethane ligand complexes.[20,21]

Low-temperature N.M.R. Solution Studies of [$PtXMe_3(MeSCH_2CH_2SEt)$].—In organic solvents, these complexes exist as a mixture of four invertomer pairs, DL-1 to DL-4 (Figure 1). The relative populations of these species were readily obtained from their ^{195}Pt-{^{1}H} spectra. Chemical shift and invertomer population data are contained in Table 4. The shifts show the expected halogen dependence, with movement to lower frequency on replacing Cl by Br or I.[4,22,23] Comparison of the shifts with the corresponding invertomers of [$PtXMe_3(MeSCH_2CH_2SMe)$] (X = Cl or I)[7] reveals that the signals are displaced to slightly higher frequencies, a trend compatible with some overall weakening of Pt–S bonding.[24] Comparison of the invertomer populations with those obtained for 2,5-dithiahexane complexes (Table 4) reveals very similar trends. For the chloro complexes, the DL-1 or *meso*-1 invertomer with both alkyl groups directed away from the axial methyl group is most populous, with the DL-3/*meso*-2 invertomer being the least favoured. On increasing the steric bulk of the halogen, the invertomers containing an *anti* orientation of alkyl groups are favoured at the expense of the DL-1/*meso*-1 invertomer, with a concomitant small increase in the DL-3/*meso*-2 population. These trends suggest that thioalkyl–axial methyl non-bonded interactions are more important than thioalkyl–halogen interactions.

It is very pertinent to note that, in the case of [$PtClMe_3(MeSCH_2CH_2SEt)$], platinum-195 studies indicate that the complex exists preferentially in $CDCl_3$ solution as the DL-1 invertomer, whereas the *X*-ray crystal structure is analogous to the DL-4 species. In previous cases, where both solid-state and solution structures were known,[4,20,21,25] the solid-state structure has invariably closely resembled the most populous invertomer in solution. It is not clear why this situation should not prevail in the present case, where clearly the crystal packing forces must be more significant than the invertomer ground-state energy differences.

Proton-decoupled ^{13}C spectra have been recorded for all three complexes at −30 °C and the data are collated in Tables 5 and 6. Signal assignments of the spectrum of [$PtClMe_3(MeSCH_2CH_2SEt)$] are given in Figures 3—5. Signals due to the low-population DL-3 invertomer were detected in only a limited number of cases.

In the platinum-methyl region (Figure 4) signals were assigned according to the known invertomer populations and ^{1}J(PtC) values where $^{1}J(PtC_{ax}) > {}^{1}J(PtC_{eq})$.[4,22] Several very consistent trends may be noted in Tables 5 and 6. Methyl carbon shifts follow the variation δ(Cl) > δ(Br) > δ(I) for

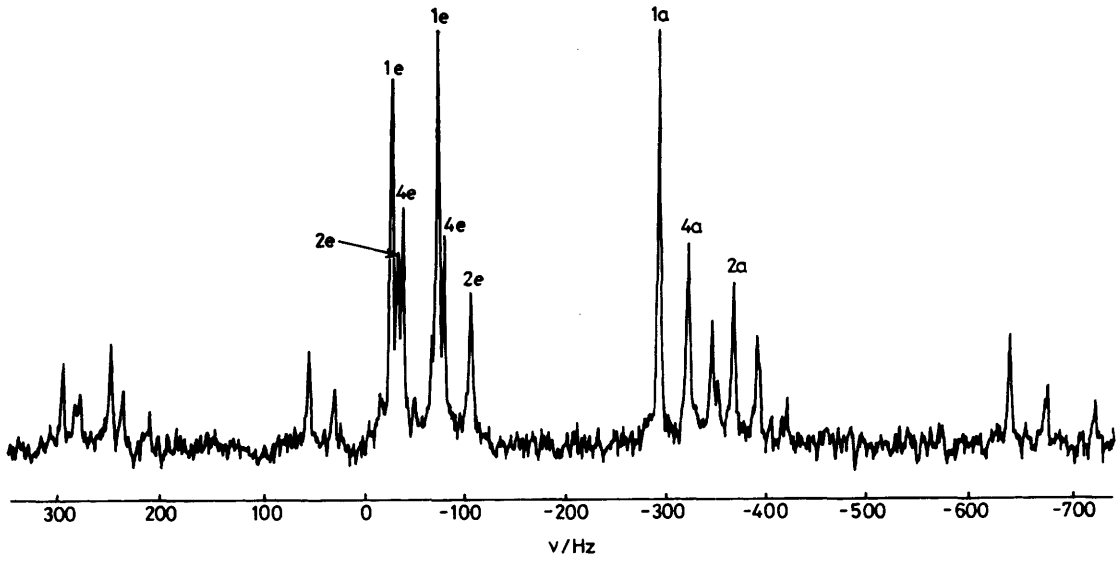

Figure 3. Platinum-methyl region of $^{13}C-\{^1H\}$ spectrum of $[PtClMe_3(MeSCH_2CH_2SEt)]$ in $CDCl_3$ at −30 °C. The numbered lines refer to the appropriate DL invertomer (a = axial, e = equatorial Pt-methyl). All unlabelled lines are ^{195}Pt satellites

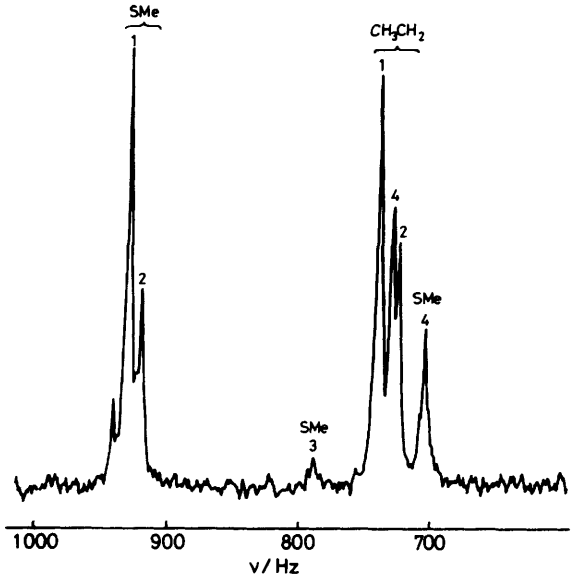

Figure 4. Ligand-methyl region of the $^{13}C-\{^1H\}$ spectrum of $[PtClMe_3(MeSCH_2CH_2SEt)]$ in $CDCl_3$ at −30 °C. The numbers refer to the appropriate DL invertomer

equatorial Pt-methyls (*trans* S), whereas the reverse trend occurs for axial Pt-methyls (*trans* X). This results in a cross-over of Pt-methyl chemical shifts in going from X = Cl (Figure 4) where $\delta(PtC_{eq}) > \delta(PtC_{ax})$ through X = Br where $\delta(PtC_{eq}) \approx \delta(PtC_{ax})$ to X = I where $\delta(PtC_{eq}) < \delta(PtX_{ax})$. The small invertomer dependence of shifts is such that for axial and equatorial methyl carbons (*trans* SEt) the order is δ(DL-1) > δ(DL-4) > δ(DL-2) whereas for equatorial methyl carbons (*trans* SMe) the order is δ(DL-1) > δ(DL-2) > (DL-4). The values of $^1J(PtC)$ follow the expected *trans* influence series[26] with $^1J(trans\ Cl) > {}^1J(trans\ Br) > {}^1J(trans\ I)$. Additionally, values of $^1J(trans\ X)$ were invariably greater than $^1J(trans\ S)$, reflecting the greater *trans* influence of S-alkyl groups relative to halogens. The invertomer dependence of $^1J(PtC)$ values was in the order DL-1 < DL-2 ≈ DL-4 for axial (*trans* X) carbons, and DL-1 > DL-2 ≈ DL-4 for equatorial (*trans* S), implying weaker Pt–S and stronger Pt–C (*trans* S) bonding in DL-1 compared to the other invertomers.

In the ligand-methyl regions of the spectra, assignments were based on a series of selective proton decoupling and DEPT experiments.[27] The S-methyl signals exhibited a much larger invertomer dependence than the SCH_2CH_3 signals (Figure 4). The methylene region of the spectra (Figure 5) comprises signals due to the SCH_2CH_3 carbons and the ligand backbone CH_2SEt and CH_2SMe carbons, in increasing order of chemical shifts. The signals due to backbone methylene and SCH_2CH_3 carbons are essentially halogen independent, whereas the SMe carbons are strongly halogen dependent, showing a marked high-frequency shift of the DL-1 and DL-2 signals on going from Cl to Br to I. When the SMe group is directed away from the halogen in the DL-3 and DL-4 invertomers, the chemical shifts are essentially unchanged. A similar halogen dependence was observed for the SCH_2CH_3 carbons in the DL-1 and DL-4 invertomers. Table 6 gives certain $^2J(PtC)$ and $^3J(PtC)$ values, having magnitudes in the ranges 6.6—9.1 and 4.6—6.9 Hz, respectively.

The foregoing analyses of the ^{195}Pt and ^{13}C spectra of $[PtXMe_3(MeSCH_2CH_2SEt)]$ have revealed remarkably consistent trends in the chemical shift and scalar coupling constant data, indicating that these parameters are excellent probes of the ground-state electronic structures of these invertomer mixtures at low temperatures. The same cannot be said about the ^1H spectra, which show severe overlaps of the methylene and thiomethyl signals, and between the equatorial platinum-methyl and SCH_2CH_3 signals.[8] No detailed assignments of these low-temperature spectra were attempted. At higher temperatures (*ca.* 60 °C) the spectra could be more completely assigned in terms of an averaged set of invertomers due to rapid sulphur inversion. The data obtained (Table 7) were compatible with the data for the $[PtXMe_3(MeSCH_2CH_2SMe)]$ series.[1,2,7]

Trimethylplatinum Halide Derivatives of 6,6-Dimethyl-2,5-dithiaheptane.—This series of complexes was prepared to

Table 7. Hydrogen-1 n.m.r. parameters (δ)[a] for complexes $[PtXMe_3(MeSCH_2CH_2SEt)]$ in $CDCl_3$ at 60 °C

X	Axial Pt–Me[a]	Equatorial Pt–Me[a] (*trans*-SMe)	Equatorial Pt–Me[a] (*trans*-SEt)	SCH_2CH_3[b]	SMe[c]	SCH_2CH_3 and SCH_2CH_3[d]
Cl	0.76 (73.1)	1.21 (70.0)	1.26 (70.2)	1.35 (14.9)	2.43	2.87—3.13
Br	0.85 (72.3)	1.32 (70.4)	1.36 (70.4)	1.34 (14.9)	2.47	2.89—3.15
I	0.97 (69.7)	1.49 (71.1)	1.53 (71.1)	1.33 (14.8)	2.54	2.86—3.14

[a] Values in parentheses are ^2J(PtH)/Hz. [b] Values in parentheses are ^3J(HH)/Hz. [c] Signals broad; ^{195}Pt satellites not resolved. [d] Severe signal overlap in this region.

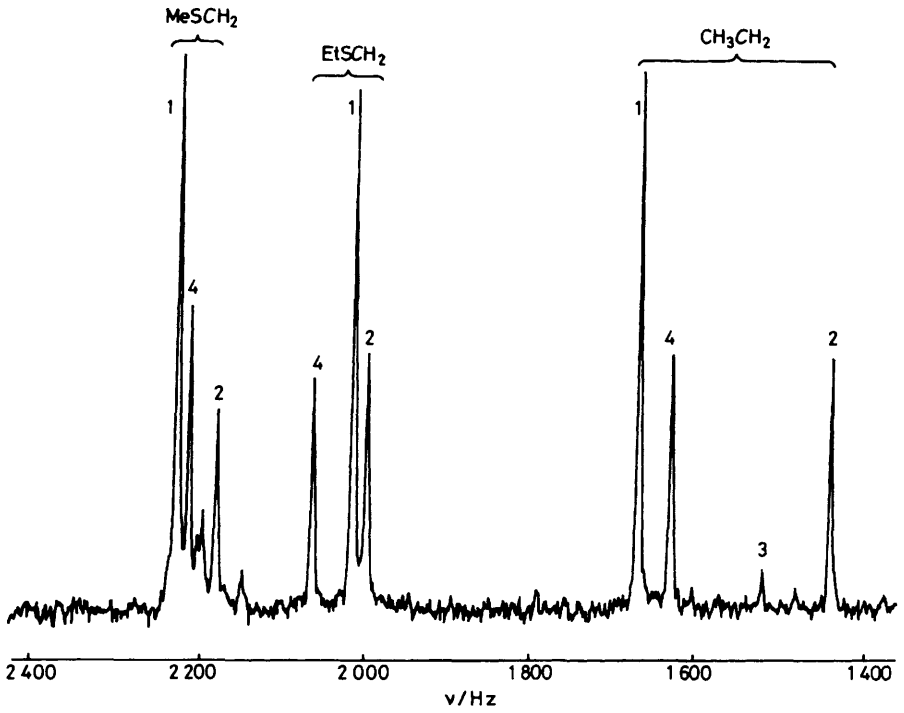

Figure 5. Methylene region of the ^{13}C-{^1H} spectrum of $[PtClMe_3(MeSCH_2CH_2SEt)]$ in $CDCl_3$ at −30 °C. The numbers refer to the appropriate DL invertomer

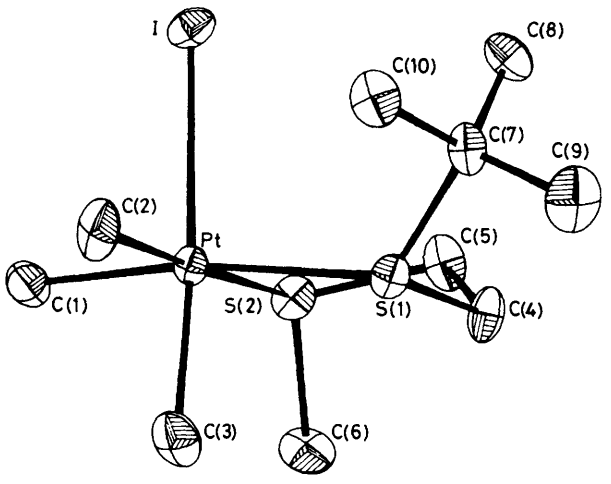

Figure 6. Crystal structure of *fac*-$[PtIMe_3(MeSCH_2CH_2SBu^t)]$ showing the atomic labelling

examine the influence of a bulky t-butyl group on the invertomer populations, the ^{195}Pt and ^{13}C chemical shift and scalar coupling constant parameters, and the pyramidal sulphur inversion energies, in these Pt^{IV} complexes.

X-*Ray Crystal Structure of fac*-$[PtIMe_3(MeSCH_2CH_2SBu^t)]$.—The structure of this complex is shown in Figure 6; fractional atomic co-ordinates and selected bond lengths and angles are given in Tables 8 and 9. Of foremost note is the *anti* arrangement of the thioalkyl groups with respect to the chelate ring, with the bulky t-butyl group directed towards the iodide ligand. This structure is closely related to the DL-4 solution structure (Figure 1). In the crystal structure the two Pt–S bond lengths are markedly different (Pt–SBu^t 2.479, Pt–SMe 2.433 Å), implying weaker Pt–S bonding in the former case. This trend is also reflected in the Pt–C bond lengths, with Pt–C(1) (*trans* SBu^t) being 2.060 Å compared to Pt–C(2) (*trans* SMe) at 2.081 Å. The Pt–SMe bond length is slightly shorter than the corresponding bond in $[PtClMe_3(MeSCH_2CH_2SEt)]$, implying stronger Pt–Me bonding in the present complex. The latter shows more severe distortions from octahedral symmetry than

does the dithiaheptane complex. For instance, the S(1)–Pt–I bond angle is increased to 99.1°, as a direct result of the non-bonded interactions between the t-butyl and iodide groups. For comparison, the S(1)–Pt–Cl angle in $[PtClMe_3(MeSCH_2CH_2SEt)]$ was 93.4°. The C(3)–Pt–S(2) angle is also large at 95.9°. Evidence for a distortion of the structure to accommodate interactions between the t-butyl group and the Pt–methyl (*trans* SMe) comes from the C–Pt–S angles. In the present complex, the C(2)–Pt–S(1) angle is 95.4 compared to 93.7° in the dithiaheptane complex, whereas the C(1)–Pt–S(2) angle is smaller (90.7 *vs.* 92.3°). This greater distortion is also reflected in the C(1)–Pt–S(1) angles (171.1 compared to 176.4°). The C(2)–Pt–S(2) angles are similar in each complex at *ca.* 177°, whereas the C(3)–Pt–I angle in the present complex is smaller than the C(3)–Pt–Cl angle in the dithiaheptane complex (175.5 *vs.* 178.6°) again presumably as a result of the steric requirements of the t-butyl group.

Considering the bond angles around sulphur, while the C(ligand backbone)–S–Pt angles are close to normal tetrahedral values, the C(ligand backbone)–S–C(alkyl) angles are 100.8 (SMe) and 104.1° (SBu^t), and the C(alkyl)–S–Pt angles are 111.0 (SMe) and 124.3° (SBu^t). There is thus a much greater distortion from tetrahedral geometry towards a planar geometry for the S–Bu^t sulphur compared to the S–Me sulphur. Such a distortion would be expected to provide easier access to the planar transition state associated with pyramidal sulphur inversion, and therefore lead to a markedly lower inversion barrier for the S–Bu^t sulphur compared to the S–Me sulphur. Solution dynamic n.m.r. studies lend support to this conclusion (see later).

Table 8. Fractional atomic co-ordinates ($\times 10^4$) for *fac*-$[PtIMe_3(MeSCH_2CH_2SBu^t)]$

Atom	*x*	*y*	*z*
Pt	8 259.7(2)	6 793.2(3)	612.4(2)
I	6 182.5(4)	8 156.2(6)	−224.2(4)
S(1)	7 852(2)	4 130(2)	−155(1)
S(2)	7 615(2)	5 703(2)	1 751(1)
C(1)	8 802(7)	8 832(10)	1 412(6)
C(2)	8 754(7)	7 832(9)	−371(7)
C(3)	9 833(7)	5 966(11)	1 269(7)
C(4)	7 443(7)	2 991(9)	671(6)
C(5)	6 869(7)	3 973(9)	1 135(5)
C(6)	8 710(7)	4 780(11)	2 710(6)
C(7)	6 731(6)	3 736(9)	−1 330(6)
C(8)	5 602(6)	3 878(10)	−1 338(6)
C(9)	6 923(8)	2 064(11)	−1 616(7)
C(10)	6 919(7)	4 966(10)	−1 979(6)

Low-temperature N.M.R. Solution Studies of $[PtXMe_3(MeSCH_2CH_2SBu^t)]$.—Proton-decoupled ^{195}Pt spectra at −70 °C gave the chemical shift and invertomer population data in Table 10. The shifts are invariably to higher frequency of those obtained for the dithiaheptane (Table 4) and dithiahexane complexes,[7] suggesting weaker overall Pt–S bonding. The ordering of the ^{195}Pt shifts is different, with DL-4 < DL-3 < DL-1 < DL-2 compared to DL-3 < DL-4 < DL-2 < DL-1 in the dithiaheptane series (Table 4). The trends in invertomer populations are as reported for other Pt^{IV} chelate complexes.[1,2,7] The present complexes show a generally greater preference for *anti* invertomers (*viz.* DL-2 and DL-4) than do the dithiaheptane complexes, reflecting the increased S-alkyl ··· S-alkyl non-bonded interactions. The DL-4 species is the more populous of the *anti* invertomers and is the most populous of all four invertomers in the bromide and iodide complexes. It is particularly noteworthy that the *X*-ray crystal structure of the latter complex closely resembles the DL-4 structure which is almost 50% abundant in $CDCl_3$ solution. This finding is in contrast to the solid-state and solution structures of $[PtClMe_3(MeSCH_2CH_2SEt)]$, reported above.

Proton-decoupled ^{13}C spectra of the chloride and bromide complexes were obtained, but the lower solubility of the iodide complex precluded the collection of any reliable data. Carbon shift and Pt–C coupling constant data for the DL-1, DL-2, and DL-4 invertomers are collected in Table 11. In general, the trends are consistent with those observed for the dithiaheptane complexes. The chemical shifts of the quaternary carbon and methylene carbon signals show only a slight halogen dependence, whereas the S-methyl carbons (DL-1, DL-2), in which the SMe group is directed towards the halogen, show strong halogen dependence. In the platinum-methyl region of the spectrum the assignment of the equatorial methyl carbons was less certain on account of the similar populations of two of the invertomer species. The assignments given in Table 11 were

Table 10. ^{195}Pt-$\{^1H\}$ chemical shifts (δ)[a] and invertomer populations (p)[b] of $[PtXMe_3(MeSCH_2CH_2SBu^t)]$

	DL-1		DL-2		DL-3		DL-4	
X	δ	*p*	δ	*p*	δ	*p*	δ	*p*
Cl	1 426.5	39.4	1 429.4	21.8	1 420.6	3.9	1 414.7	34.9
Br	1 308.0	25.9	1 322.0	24.3	1 294.6	6.6	1 274.2	43.2
I	1 085.5	15.8	1 133.0	25.7	1 079.4	11.3	1 020.8	47.2

[a] In CD_2Cl_2 solvent at 203 K; shifts relative to ^{195}Pt Ξ = 21.4 MHz. [b] Percentage populations at 203 K.

Table 9. Bond lengths (Å) and angles (°) for *fac*-$[PtIMe_3(MeSCH_2CH_2SBu^t)]$*

(*i*) Bond lengths

I–Pt	2.784(4)	S(1)–Pt	2.479(4)	C(5)–S(2)	1.797(9)	C(6)–S(2)	1.785(10)
S(2)–Pt	2.433(4)	C(1)–Pt	2.060(10)	C(5)–C(4)	1.490(12)	C(8)–C(7)	1.505(12)
C(2)–Pt	2.081(10)	C(3)–Pt	2.047(10)	C(9)–C(7)	1.519(13)	C(10)–C(7)	1.530(12)
C(4)–S(1)	1.847(10)	C(7)–S(1)	1.863(10)				

(*ii*) Bond angles

S(1)–Pt–I	99.1(1)	S(2)–Pt–I	85.2(1)	C(7)–S(1)–Pt	124.3(4)	C(4)–S(1)–Pt	101.4(4)
S(2)–Pt–S(1)	86.6(2)	C(1)–Pt–I	89.1(3)	C(5)–S(2)–Pt	101.3(4)	C(7)–S(1)–C(4)	104.1(5)
C(1)–Pt–S(1)	171.1(2)	C(1)–Pt–S(2)	90.7(4)	C(6)–S(2)–C(5)	100.8(5)	C(6)–S(2)–Pt	111.0(4)
C(2)–Pt–I	92.1(3)	C(2)–Pt–S(1)	95.4(3)	C(4)–C(5)–S(2)	114.7(7)	C(5)–C(4)–S(1)	113.9(6)
C(2)–Pt–S(2)	176.9(2)	C(2)–Pt–C(1)	87.7(5)	C(9)–C(7)–S(1)	106.6(7)	C(8)–C(7)–S(1)	113.5(7)
C(3)–Pt–I	175.5(2)	C(3)–Pt–S(1)	85.3(3)	C(10)–C(7)–S(1)	104.3(6)	C(9)–C(7)–C(8)	110.9(8)
C(3)–Pt–S(2)	95.9(4)	C(3)–Pt–C(1)	86.5(4)	C(10)–C(7)–C(9)	109.5(8)	C(10)–C(7)–C(8)	111.8(8)
C(3)–Pt–C(2)	86.7(5)						

* Values in parentheses are the standard deviations of the least significant figure.

Table 11. Carbon-13 n.m.r. parameters[a] for complexes $[PtXMe_3(MeSCH_2CH_2SBu^t)]$ in CD_2Cl_2

X	Invertomer	Axial Pt–Me	Equatorial Pt–Me (*trans* SBu^t)	Equatorial Pt–Me (*trans* SMe)	SMe	$SC(CH_3)_3$	$SC(CH_3)_3$	CH_2SBu^t	$MeSCH_2$
Cl[b]	DL-1	−2.08 (690.5)	3.79 (647.0)	2.06 (634.8)	16.41	29.61	52.41 (11.9)	30.46	40.69
	DL-2	−5.54 (696.6)	2.38 (636.9)	−0.10 (629.3)	16.00	30.11	50.30 (—)	31.97	39.14
	DL-4	−2.45 (699.2)	0.95 (636.3)	2.44 (628.0)	12.90	29.75	52.50 (12.1)	31.35	39.78
Br[c]	DL-1	2.62 (686.3)	3.46 (642.1)	1.74 (633.9)	18.12	29.53	52.64 (12.3)	30.40	40.84
	DL-2	−1.22 (690.1)	0.08 (630.9)	−0.70 (624.8)	18.02	30.17	50.69 (—)	31.94	39.21
	DL-4	1.94 (694.2)	1.81 (630.3)	1.30 (621.9)	12.89	29.64	52.75 (12.6)	31.37	39.88

[a] Chemical shifts (δ); values in parentheses are ^1J(PtC) (platinum-methyl signals) or ^2J(PtC) (quaternary carbon signals) in Hz. [b] At −90 °C. [c] At −80 °C. In addition to the signals given, the SMe signal for the DL-3 invertomer was observed at δ 14.19.

Table 12. Hydrogen-1 n.m.r. parameters[a] for complexes $[PtXMe_3(MeSCH_2CH_2SBu^t)]$ in $CDCl_3$ at 60 °C

X	Axial Pt–Me	Equatorial Pt–Me (*trans* SMe)	Equatorial Pt–Me (*trans* SBu^t)	$SC(CH_3)_3$	SMe[b]	SCH_2CH_2S
Cl	0.82 (72.6)	1.26 (71.4)	1.40 (70.1)	1.50	2.40	2.81—3.25
Br	0.92 (72.0)	1.38 (71.9)	1.51 (70.1)	1.52	2.47	2.82—3.29
I	1.08 (71.1)	1.53 (73.7)	1.65 (71.1)	1.50	2.51	2.83—3.25

[a] Chemical shifts (δ); values in parentheses are ^2J(PtH)/Hz. [b] Signals broad; ^{195}Pt satellites not resolved.

Table 13. ^{195}Pt-{^{1}H} N.m.r. chemical shifts (δ)[a] and invertomer populations (p)[a] of complexes $[PtXMe_3(Bu^tSCH_2CH_2SBu^t)]$[b]

	meso-1		DL		*meso*-2	
X	δ	p	δ	p	δ	p
Cl	1 477.8	47.3	1 511.1	47.5	1 507.0	5.2
Br	1 340.4	31.0	1 381.3	59.6	1 392.5	9.4
I	1 084.1	16.8	1 151.7	68.2	1 200.6	15.0

[a] At 203 K; shifts relative to ^{195}Pt Ξ = 21.4 MHz. [b] In CD_2Cl_2 solution.

based on the assumptions that (*i*) ^1J(PtC) values were in the order DL-1 > DL-2 > DL-4, a trend similar to that noted for the corresponding dithiaheptane complexes, and (*ii*) for each invertomer ^1J(PtC) (*trans* SBu^t) > ^1J(PtC) (*trans* SMe).

Hydrogen-1 spectra were also recorded at *ca.* −90 °C but in general were not very informative due to their complexity. Spectra recorded at 60 °C were consistent with rapid sulphur inversion and parameters for these fast-exchange spectra are reported in Table 12.

Trimethylplatinum(IV) *Halide Derivatives of* 2,2,7,7-*Tetramethyl*-3,6-*dithiaoctane*.—At low temperatures these complexes exist in solution as a mixture of *meso*-1, *meso*-2, and DL-1/2 invertomers, analogous to 2,5-dithiahexane complexes.[1,2,22] Platinum-195 shifts and invertomer populations are presented in Table 13. Comparison of the shifts with those for corresponding dithiahexane complexes reveals high-frequency shifts of 130—160 p.p.m. The dependence of ^{195}Pt shifts on the steric bulk of the ligand has been noted previously[28] and is illustrated by the three pairs of complexes *trans*-$[PtCl_2(AsR_3)_2]$,[29] $[PtCl_2(CO)R]^-$ (R = Et or Pr^i),[30] and *trans*-$[PtCl_2(NHMeR)(C_2H_4)]$ (R = Me or Pr^i).[31] The ^{195}Pt shifts also exhibit the well established halogen dependence.[23,28] The invertomer populations exhibit the same halogen dependence as in the dithiahexane complexes,[2] with the DL population and, to a lesser extent, the *meso*-2 population increasing at the expense of *meso*-1, on increasing halogen size. There is, however, a generally greater preference for DL invertomers over *meso* invertomers for the present complexes compared to $[PtXMe_3(MeSCH_2CH_2SMe)]$.

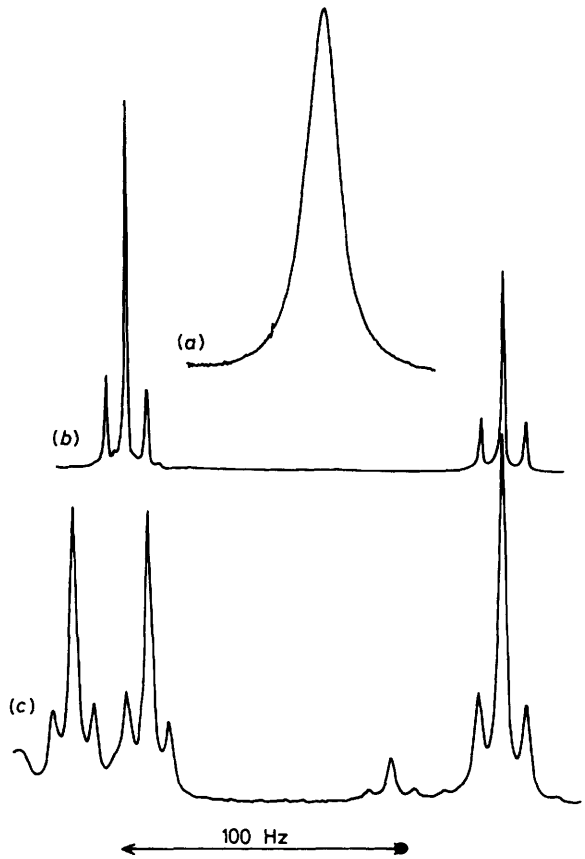

Figure 7. Hydrogen-1 spectra of $[PtBrMe_3(MeSCH_2CH_2SBu^t)]$ in $CDCl_3$ showing the SMe signals at (*a*) 60 °C, (*b*) −10 °C, and (*c*) −80 °C

Proton-decoupled ^{13}C spectra were obtained at −90 and 30 °C for the three complexes $[PtXMe_3(Bu^tSCH_2CH_2SBu^t)]$ (X = Cl, Br, or I), and the data are collected in Table 14. All the assignments are reasonably unambiguous and the chemical shift changes with halogen quite predictable. The trends in ^2J(PtC) values help greatly in assigning the quaternary carbon signals. For example, in the case of $[PtIMe_3(Bu^tSCH_2CH_2SBu^t)]$, the *meso*-1 signal (δ 52.25) showed a ^2J(PtC) value of 13.9 Hz compared to the *meso*-2 signal (δ 51.17) with a ^2J(PtC) value of 6.9 Hz. Using these data, the two signals due to the DL invertomers at δ 52.52 [^2J(PtC) = 13.2 Hz] and 51.54

Table 14. Carbon-13 n.m.r. parameters[a] for complexes $[PtXMe_3(Bu^tSCH_2CH_2SBu^t)]$ in CD_2Cl_2

X	T/°C	Invertomer	Axial Pt–Me	Equatorial Pt–Me	$SC(CH_3)_3$[b]	SCH_2CH_2S	$SC(CH_3)_3$
Cl	−90	*meso*-1	−4.46 (696.2)	5.25 (646.8)		32.57	52.13 (12.8)
				4.60 (638.3)		35.18	52.30 (11.8)
		DL	−0.40 (693.1)		29.77, 30.10		
				2.76 (629.0)		34.69	50.53[c]
		meso-2[d]					
	30		−2.69 (691.9)	4.71 (653.2)	30.23	32.64	51.66 (10.6)
Br	−90	*meso*-1	1.86[c]	4.72 (642.5)		32.67	52.30 (13.0)
				3.59 (631.5)		35.53	52.53 (12.1)
		DL	0.00 (691.2)		29.72, 30.19		
				2.43 (629.7)		34.87	50.91 (4.2)
		meso-2	0.42[c]	4.38[c]		33.10	50.64[c]
	30		1.37 (690.7)	4.03 (646.4)	30.26	32.96	51.81 (10.6)
I	−90	*meso*-1	11.75 (666.7)	3.33 (636.8)		32.90	52.25 (13.9)
				1.61 (625.8)		36.05	52.52 (13.2)
		DL	6.51 (669.8)		29.50, 30.34		
				1.37 (622.6)		34.95	51.54 (6.3)
		meso-2	3.25 (672.9)	0.36 (622.6)		33.91	51.17 (6.9)
	30		7.34 (669.0)	2.38 (636.5)	30.24	33.61	51.90 (10.7)

[a] Chemical shifts (δ); values in parentheses are ^nJ(PtC)/Hz [n = 1 for Pt–Me resonances, n = 2 for $C(CH_3)_3$ resonances]. [b] See text. [c] ^{195}Pt Satellites not observed. [d] Signals not observed for *meso*-2 invertomer.

Table 15. Hydrogen-1 n.m.r. parameters[a] for complexes $[PtXMe_3(Bu^tSCH_2CH_2SBu^t)]$ in CD_2Cl_2 at 20 °C

X	Axial Pt–Me	Equatorial Pt–Me	$C(CH_3)_3$	SCH_2CH_2S[b]
Cl	0.78 (71.7)	1.41 (71.6)	1.51	2.92—3.29
Br	0.97 (71.7)	1.51 (71.8)	1.51	2.95—3.31
I	1.21 (70.2)	1.69 (72.2)	1.49	3.01—3.33

[a] Chemical shifts (δ); values in parentheses are ^2J(PtH)/Hz. [b] AA'BB' multiplets were observed in each case.

Table 16. Sulphur inversion energies [$\Delta G^‡$ (243 K)/kJ mol^{-1}] for complexes $[PtXMe_3L]$ (X = Cl, Br, or I)

		X		
L	SR	Cl	Br	I
$MeSCH_2CH_2SMe$	SMe	64.0 ± 0.16[a]		63.2 ± 0.13
	SMe	62.6 ± 0.26[b]		
$MeSCH_2CH_2SEt$	SEt	61.3 ± 0.03[c]	61.6 ± 0.03	61.4 ± 0.03
	SMe	62.5 ± 1.2[d]	64.0 ± 2.2	63.9 ± 1.2
	SEt	56.1 ± 0.49[e]	57.7 ± 0.36	59.2 ± 0.27
	SMe	64.5 ± 0.94[f]	65.2 ± 2.2	64.4 ± 1.2
$MeSCH_2CH_2SBu^t$	SBu^t	46.05 ± 0.10[c]		45.14 ± 0.25
	SBu^t	46.05 ± 0.41[e]		46.57 ± 0.14
	SMe	62.68 ± 0.56[g]		65.15 ± 0.18
$Bu^tSCH_2CH_2SBu^t$	SBu^t			43.33 ± 0.17[h]

[a] *meso*-1 ⟶ DL. [b] DL ⟶ *meso*-2. [c] DL-1 ⟶ DL-2. [d] DL-2 ⟶ DL-3. [e] DL-3 ⟶ DL-4. [f] DL-1 ⟶ DL-4. [g] ⟨DL-1/2⟩ ⟶ ⟨DL-3/4⟩. [h] *meso*-1 ⟶ DL or DL ⟶ *meso*-2.

[^2J(PtC) = 6.3 Hz] could be unambiguously assigned to the quaternary Bu^t carbons *cis* to axial halogen and *cis* to axial methyl, respectively. Values of ^1J(PtC) showed clear *trans* influence dependencies,[22] but no clear dependence on invertomer. Values of ^1J(PtC) (*trans* S) were generally somewhat greater for *meso*-1 than *meso*-2, implying stronger Pt–C and weaker Pt–S bonds in the former species. The pairs of methyl carbon signals for the DL invertomer could be individually assigned on this basis. Values of ^1J(PtC) (*trans* X) are smaller for the present complexes compared to the dithiahexane complexes, whereas the reverse trend is observed for ^1J(PtC) (*trans* S) values, implying weaker Pt–S bonding of the Bu^t-substituted ligands.

Hydrogen-1 spectra were recorded for all three complexes at −90 and 20 °C. At the lower temperatures, considerable overlapping of signals was found, and only the ambient-temperature spectra were analysed (Table 15). These data are consistent with rapid interconversion of the invertomers *via* sulphur inversion, and their halogen and invertomer dependencies are in general analogous to the ^{13}C-{^1H} data.

Dynamic N.M.R. Experiments.—(*i*) *At low temperature.* The solution fluxionalities of these platinum(IV) complexes have been examined by one-dimensional bandshape and/or two-dimensional EXSY n.m.r. experiments as appropriate.

In the case of the $[PtXMe_3(MeSCH_2CH_2SEt)]$ complexes, only the 2D-EXSY method was capable of handling the sulphur inversion problem, since the spectra were sensitive to four independent rate constants. The case of $[PtIMe_3(MeSCH_2CH_2SEt)]$ has been described in detail recently.[8] Similar analyses were performed on the chloride and bromide complexes but these studies were restricted to a single temperature (243 K) in view of the considerable experimental time involved in recording ^{195}Pt 2D-EXSY spectra; energy data are expressed in terms of $\Delta G^‡$ (243 K) values. These are given in Table 16 for the four distinct invertomer interconversion processes, two of which involve S-methyl inversion and two involving S-ethyl inversion.

It was originally intended to examine the complexes $[PtXMe_3(MeSCH_2CH_2SBu^t)]$ in a similar way, using ^{195}Pt 2D-EXSY experiments. However, it became apparent that the rates of inversion of S–Me and S–Bu^t groups were sufficiently different for the two processes to be treated independently. This was due to the fact that on increasing temperature the rate of S–Bu^t inversion became fast on the n.m.r. time-scale before any observable onset of S–Me inversion. This meant that the dynamic problem could be conveniently handled by one-dimensional bandshape analysis, rather than resorting to two-dimensional methods. The spectral changes associated with the SMe signals of $[PtBrMe_3(MeSCH_2CH_2SBu^t)]$ are shown in Figure 7. At −80 °C, separate signals due to the four DL invertomers are seen. In contrast, at −10 °C, DL-1 ⇌ DL-2 and DL-3 ⇌ DL-4 interconversions due to S–Bu^t inversion

Table 17. Arrhenius and Eyring activation parameters for sulphur inversion in complexes $[PtXMe_3(MeSCH_2CH_2SBu^t)]$

X	Inversion process	E_a/kJ mol^{-1}	$\log_{10}$ (A/s^{-1})	$\Delta H^{\ddagger}$/kJ mol^{-1}	$\Delta S^{\ddagger}$/J K^{-1} mol^{-1}	$\Delta G^{\ddagger}$ (298 K)/kJ mol^{-1}
Cl	DL-1 ⟶ DL-2	60.49 ± 1.07	15.80 ± 0.25	58.64 ± 1.07	51.8 ± 4.8	43.21 ± 0.36
	DL-3 ⟶ DL-4	58.84 ± 3.54	15.45 ± 0.85	57.03 ± 3.55	45.2 ± 16.3	43.56 ± 1.31
	DL-1/2 ⟶ DL-3/4	66.50 ± 2.85	13.51 ± 0.49	63.99 ± 2.84	5.4 ± 9.4	62.39 ± 0.04
I	DL-1 ⟶ DL-2	54.75 ± 1.87	14.77 ± 0.46	52.99 ± 1.86	32.3 ± 8.7	43.37 ± 0.73
	DL-3 ⟶ DL-4	55.66 ± 1.07	14.66 ± 0.26	53.88 ± 1.05	30.1 ± 4.9	44.90 ± 0.40
	DL-1/2 ⟶ DL-3/4	75.25 ± 0.74	14.86 ± 0.12	72.61 ± 0.76	30.7 ± 2.4	63.47 ± 0.04

Table 18. Activation energies[a] for platinum-methyl fluxions in $[PtXMe_3L]$ complexes

L	X	eq_1–ax	eq_2–ax	eq_1–eq_2	Ref.
$MeSCH_2CH_2SEt$	Cl	96.3 ± 0.9	93.9 ± 0.6	100.4 ± 0.7	This work
	I	92.6 ± 0.4	90.9 ± 0.5	97.7 ± 1.9	8
$MeSCH_2CH_2SBu^t$	Cl	89.5 ± 1.2	80.8 ± 0.4	89.3 ± 0.8	This work
$MeSCH_2CH_2SMe$	I	89.6 ± 0.3	89.6 ± 0.3	*b*	*c*
o-$MeSC_6H_4SMe$	Cl	83.8 ± 1.8	83.8 ± 1.8	*b*	5
$MeSCH_2SCH_2SMe$	Cl	79.2 ± 0.2	79.2 ± 0.2	*b,d*	6

[a] Expressed as $\Delta G^{\ddagger}$ (298 K)/kJ mol^{-1} values. [b] Spectra insensitive to this exchange. [c] Unpublished work. [d] Effective eq_1–eq_2 exchange occurs as a result of ligand rotation for which $\Delta G^{\ddagger}$ (298 K) = 77.7 ± 0.3 kJ mol^{-1}, measured from ligand methylene region of spectrum.

are rapid, but S–Me inversions are slow producing two distinct exchange-averaged invertomers. By 60 °C, both sulphurs are inverting rapidly and a single exchange-averaged SMe signal is detected. Bandshape fittings were performed in the usual way on the chloride and iodide complexes, and the full energy data are given in Table 17. The $\Delta G^{\ddagger}$ (298 K) data were converted to $\Delta G^{\ddagger}$ (243 K) values (Table 16) for comparison with data for the other Pt^{IV} complexes.

Sulphur inversion in the $[PtXMe_3(Bu^tSCH_2CH_2SBu^t)]$ complexes manifests itself in an interconversion of the low-temperature *meso*-1, DL, and *meso*-2 invertomers. This type of dynamic problem has been studied extensively for 2,5-dithiahexane complexes.[2] As there is virtually no halogen dependence of the sulphur inversion barriers, the present study was restricted to $[PtIMe_3(Bu^tSCH_2CH_2SBu^t)]$. Proton bandshape analysis gave the following energy data, E_a = 63.01 ± 1.50 kJ mol^{-1}, $\log_{10}$ (A/s^{-1}) = 16.93 ± 0.36, $\Delta H^{\ddagger}$ = 61.19 ± 1.51 kJ mol^{-1}, $\Delta S^{\ddagger}$ = 73.5 ± 6.9 J K^{-1} mol^{-1}, and $\Delta G^{\ddagger}$ (298 K) = 39.29 ± 0.54 kJ mol^{-1}. The latter parameter was converted to $\Delta G^{\ddagger}$ (243 K) and included in Table 16.

(*ii*) *At high temperature.* In our previous study[8] of $[PtIMe_3(MeSCH_2CH_2SEt)]$ the Pt-methyl ^1H signals were shown to undergo exchange at above-ambient temperatures as a result of a correlated ligand rotation/$PtMe_3$ rotation fluxion which transfers spin magnetisation between the three Pt-methyl environments at different rates. Using ^1H 2D-EXSY experiments as previously we have studied the complexes $[PtClMe_3(MeSCH_2CH_2SEt)]$ and $[PtClMe_3(MeSCH_2CH_2SBu^t)]$ to investigate any influence of different S-alkyl groups on the fluxional process. Similar studies on $[PtXMe_3(Bu^tSCH_2CH_2SBu^t)]$ proved impossible due to overlap of Bu^t and PtMe methyl signals. In the above two cases 2D-EXSY spectra were measured over somewhat limited temperatures ranges ($\Delta T \approx$ 30—40 K) and so the energy barriers for the fluxions are quoted simply as $\Delta G^{\ddagger}$ values, since these are less prone to systematic error than the $\Delta H^{\ddagger}$ and $\Delta S^{\ddagger}$ parameters. The results are given in Table 18 and are compared with values obtained previously for related platinum(IV) chelate complexes. As the latter involved ligands of higher symmetry, only a single type of axial–equatorial Pt-methyl exchange could be measured in these cases.

Discussion

The main achievements of this work can be stated as follows.

A definitive characterisation of the platinum(IV) complexes $[PtXMe_3(RSCH_2CH_2SR')]$ (X = Cl, Br, or I; R,R' = like or unlike alkyl groups) in $CDCl_3$ solution has been achieved by ^1H, ^{13}C-{^1H}, and ^{195}Pt n.m.r. experiments, at low temperatures. In the invertomer mixtures the general preference is for the S-alkyl groups in the chelate ligands to adopt an *anti* relationship (*e.g.* DL-2, DL-4) particularly with bulky groups such as S-Bu^t. The *syn* invertomer DL-3/*meso*-2 is always least abundant but in general the overall population distribution in the series depends on a sensitive balance between the thioalkyl interactions with the axial Pt-methyl and the axial halogen. Also, the invertomer populations are appreciably halogen and temperature dependent with DL-2, DL-3, and DL-4 populations increasing at the expense of DL-1 for an increase in halogen size or a decrease in solution temperature. It must be remembered that in solution the mirror-image counterparts of the DL structures DL-1 to DL-4 (Figure 1) also exist. These give identical n.m.r. spectra in achiral solvents. Interconversion between the two sets of structures can take place by 180° 'pancake' rotations of the ligand.

These do indeed occur, as we have shown, but only at temperatures where distinction between individual invertomers is lost as a result of rapid pyramidal sulphur inversion. A total graph diagram depicting the eight diastereoisomers of the complexes at the corners of a simple cube (*cf.* Figure 8, ref. 5) is therefore only of hypothetical interest.

In two cases solution and solid-state crystal structures were compared. For $[PtIMe_3(MeSCH_2CH_2SBu^t)]$ and $[PtClMe_3(MeSCH_2CH_2SEt)]$, the crystal structures in both cases corresponded to the DL-4 solution structures. This represents the most abundant invertomer in solution for the iodide complex but only the second-most abundant species in the chloride case. This serves as a reminder that crystal-packing forces may be the determining factors in solid-state structures, dominating any small differences in ground-state energies of solution species.

The *X*-ray data indicate some distortion from tetrahedral to planar geometry for the sulphur atom bearing a t-butyl group. Such a distortion leads to easier access to the planar transition state associated with sulphur pyramidal inversion, and is reflected in the relative inversion energies. These have been collected in Table 16 in the form of $\Delta G^{\ddagger}$ (243 K) values. If the relatively small effects of different halogens and invertomer ground-state energies are averaged out, the following definitive trend in S-alkyl inversion barriers is obtained: SMe (~64 kJ mol^{-1}) > SEt (~60 kJ mol^{-1}) ≫ SBu^t (~45 kJ mol^{-1}). This represents the most accurate evaluation to date of alkyl dependence of sulphur inversion barriers. It mirrors the trends, based on less extensive data, found recently[3,2] for the complexes $[W(CO)_4(RSCH_2CH_2SR)]$ (R = Me, Et, Pr^i, or Bu^t) and is in

accordance with earlier data on nitrogen pyramidal inversion.[33,34]

A further aim of this work was to elucidate a mechanism for the high-temperature fluxions in these complexes. The unsymmetrical chelate ligands allow three Pt-methyl exchange pathways to be monitored. The energies of these are given in Table 18. The data for $[PtIMe_3(MeSCH_2CH_2SEt)]$ have been rationalised earlier in terms of a strongly correlated ligand 180° 'pancake' rotation and a 120° $PtMe_3$ moiety rotation.[8] Full correlation between these processes would lead to no direct eq–eq Pt-methyl exchange (see Figure 7 of ref. 8), whereas in fact slow eq–eq exchange does occur and its associated activation energy evaluated. Energies for the corresponding chloride complex have now been evaluated (Table 18) and the data again imply a strong correlation between the ligand and $PtMe_3$ rotations. In the case of the $MeSCH_2CH_2SBu^t$ ligand complex, the fluxional energies are notable in two respects. First the ax–eq Pt-methyl exchange pathways are unequally favoured, the less preferred exchange being thought to involve the axial Pt-methyl on the SMe side of the complex. Secondly, the energy of this route is almost identical to that of the direct eq–eq exchange. The differing ax–eq exchange energies almost certainly reflect the differing Pt–SMe and Pt–SBu^t bond strengths, but precisely how this manifests itself in the overall mechanism is uncertain. A further uncertainty arises from the assignment of the two equatorial Pt-methyl environments (eq_1 and eq_2), that used in Table 18 being tentative. Further difficulties arise from the fact that the transition-state structure for this fluxion will depend on the directions of rotation of both the ligand and $PtMe_3$ moieties. In the case of the $MeSCH_2CH_2SBu^t$ ligand, these directions of rotation will not be equally preferred, and it is perhaps for this reason that the ligand-centred and $PtMe_3$-centred movements have a lower degree of correlation than in the $MeSCH_2CH_2SEt$ ligand complexes.

No information can be obtained regarding the correlation of the two dynamic processes in the case of the $MeSCH_2CH_2SMe$[2] and o-$MeSC_6H_4SMe$[5] complexes, but the energy values of ax–eq exchange (Table 18) are not unexpected, with lower values for the aromatic ligand complex showing the effects of ligand backbone unsaturation. Previous data[6] for a $MeSCH_2SCH_2SMe$ ligand complex are also included for comparison purposes. This six-membered chelate ring clearly undergoes more facile 'pancake' rotations than the five-membered chelates. However, no direct eq–eq Pt-methyl exchange can be measured in this type of symmetrical ligand complex and so again no insight is possible into any correlation between the ligand-centred and $PtMe_3$-centred dynamic processes.

Acknowledgements

We thank Dr. T. P. J. Coston for the preparation of a sample of $[PtIMe_3(MeSCH_2CH_2SMe)]$.

References

1 E. W. Abel. A. R. Khan, K. Kite, K. G. Orrell, and V. Šik, *J. Chem. Soc., Dalton Trans.*, 1980, 1169.
2 E. W. Abel, A. R. Khan, K. Kite, K. G. Orrell, and V. Šik, *J. Chem. Soc., Dalton Trans.*, 1980, 1175.
3 E. W. Abel, S. K. Bhargava, and K. G. Orrell, *Prog. Inorg. Chem.*, 1984, **32**, 1.
4 E. W. Abel, S. K. Bhargava, K. G. Orrell, A. W. G. Platt, V. Šik, and T. S. Cameron, *J. Chem. Soc., Dalton Trans.*, 1985, 345.
5 E. W. Abel, S. K. Bhargava, K. Kite, K. G. Orrell, V. Šik, and B. L. Williams, *J. Chem. Soc., Dalton Trans.*, 1982, 583.
6 E. W. Abel, M. Z. A. Chowdhury, K. G. Orrell, and V. Šik, *J. Organomet. Chem.*, 1983, **258**, 109.
7 E. W. Abel, T. P. J. Coston, K. G. Orrell, V. Šik, and D. Stephenson, *J. Magn. Reson.*, 1986, **70**, 34.
8 E. W. Abel, I. Moss, K. G. Orrell, V. Šik, and D. Stephenson, *J. Chem. Soc., Dalton Trans.*, 1987, 2695.
9 D. Welti and D. Whittaker, *J. Chem. Soc.*, 1962, 4372.
10 D. A. Kleier and G. Binsch, DNMR, Quantum Chemistry Program Exchange, Indiana University, U.S.A., 1970, Program 165.
11 M. B. Hursthouse, R. A. Jones, K. M. A. Malik, and G. Wilkinson, *J. Am. Chem. Soc.*, 1979, **101**, 4128.
12 A. C. T. North, D. C. Phillips, and F. S. Mathews, *Acta Crystallogr., Sect. A*, 1968, **24**, 351.
13 G. M. Sheldrick, SHELX-86, Program for Crystal Structure Solution, University of Göttingen, 1986.
14 G. M. Sheldrick, SHELX-76, Program for Crystal Structure Determination and Refinement, University of Cambridge, 1976.
15 D. T. Cromer and J. B. Mann, *Acta Crystallogr., Sect. A*, 1968, **24**, 321.
16 D. T. Cromer and D. Liberman, *J. Chem. Phys.*, 1970, **53**, 1891.
17 E. W. Abel, M. Booth, K. G. Orrell, G. M. Pring, and T. S. Cameron, *J. Chem. Soc., Chem. Commun.*, 1981, 29.
18 E. W. Abel, G. D. King, K. G. Orrell, V. Šik, T. S. Cameron, and K. Jochem, *J. Chem. Soc., Dalton Trans.*, 1984, 2047.
19 E. W. Abel, N. A. Cooley, K. Kite, K. G. Orrell, V. Šik, M. B. Hursthouse, and H. M. Dawes, *Polyhedron*, 1987, **6**, 1261.
20 G. M. Reisner, I. Bernal, and G. R. Dobson, *Inorg. Chim. Acta*, 1981, **50**, 227.
21 E. N. Baker and N. G. Larsen, *J. Chem. Soc., Dalton Trans.*, 1976, 1769.
22 E. W. Abel, K. G. Orrell, and A. W. G. Platt, *J. Chem. Soc., Dalton Trans.*, 1983, 2345.
23 P. S. Pregosin, *Annu. Rep. NMR Spectrosc.*, 1986, **17**, 285.
24 P. L. Goggin, R. J. Goodfellow, S. R. Haddock, B. F. Taylor, and I. R. H. Marshall, *J. Chem. Soc., Dalton Trans.*, 1976, 459.
25 D. E. Halverson, G. M. Reisner, G. R. Dobson, I. Bernal, and T. L. Mulcahy, *Inorg. Chem.*, 1982, **21**, 4285.
26 T. G. Appleton, H. C. Clark, and L. E. Manzer, *Coord. Chem. Rev.*, 1973, **10**, 335.
27 D. M. Doddrell, D. T. Pegg, and M. R. Bendall, *J. Magn. Reson.*, 1982, **48**, 323.
28 P. S. Pregosin, *Coord. Chem. Rev.*, 1982, **44**, 247.
29 G. Balimann, Ph.D. Thesis, Eidgenössische Technische Hochschule, Zurich, 1977.
30 J. Browning, P. L. Goggin, R. J. Goodfellow, N. W. Hurst, L. G. Mallinson, and M. Murray, *J. Chem. Soc., Dalton Trans*, 1978, 872.
31 P. S. Pregosin, S. N. Sze, P. Salvadori, and R. Lazzaroni, *Helv. Chim. Acta*, 1977, **60**, 2514.
32 E. W. Abel, I. Moss, K. G. Orrell, and V. Šik, *J. Organomet. Chem.*, 1987, **326**, 187.
33 A. T. Bottini and J. D. Roberts, *J. Am. Chem. Soc.*, 1958, **80**, 5203.
34 F. A. L. Anet and J. M. Osyany, *J. Am. Chem. Soc.*, 1967, **89**, 352.

Received 13*th April* 1987; *Paper* 7/667